

## Accepted Manuscript

Studies of CDK 8/19 Inhibitors: Discovery of Novel and Selective CDK8/19 Dual Inhibitors and Elimination of Their CYP3A4 Time-Dependent Inhibition Potential

Jun Fujimoto, Takaharu Hirayama, Yasuhiro Hirata, Yukiko Hikichi, Saomi Murai, Maki Hasegawa, Yuka Hasegawa, Kazuko Yonemori, Akito Hata, Kazunobu Aoyama, Douglas R. Cary

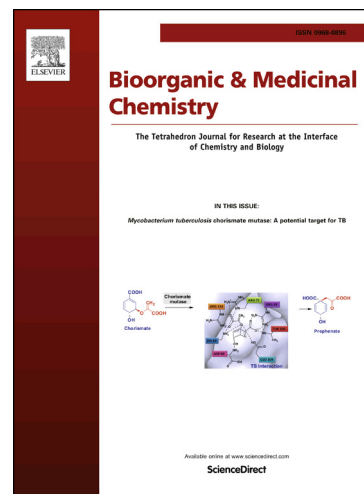
PII: S0968-0896(16)31317-7  
DOI: <http://dx.doi.org/10.1016/j.bmc.2017.03.049>  
Reference: BMC 13647

To appear in: *Bioorganic & Medicinal Chemistry*

Received Date: 21 December 2016  
Revised Date: 19 February 2017  
Accepted Date: 22 March 2017

Please cite this article as: Fujimoto, J., Hirayama, T., Hirata, Y., Hikichi, Y., Murai, S., Hasegawa, M., Hasegawa, Y., Yonemori, K., Hata, A., Aoyama, K., Cary, D.R., Studies of CDK 8/19 Inhibitors: Discovery of Novel and Selective CDK8/19 Dual Inhibitors and Elimination of Their CYP3A4 Time-Dependent Inhibition Potential, *Bioorganic & Medicinal Chemistry* (2017), doi: <http://dx.doi.org/10.1016/j.bmc.2017.03.049>

This is a PDF file of an unedited manuscript that has been accepted for publication. As a service to our customers we are providing this early version of the manuscript. The manuscript will undergo copyediting, typesetting, and review of the resulting proof before it is published in its final form. Please note that during the production process errors may be discovered which could affect the content, and all legal disclaimers that apply to the journal pertain.



**Studies of CDK 8/19 Inhibitors:  
Discovery of Novel and Selective CDK8/19 Dual Inhibitors and Elimination of Their CYP3A4  
Time-Dependent Inhibition Potential**

Jun Fujimoto<sup>a,\*</sup>, Takaharu Hirayama<sup>a</sup>, Yasuhiro Hirata<sup>a</sup>, Yukiko Hikichi<sup>b</sup>, Saomi Murai<sup>a</sup>, Maki Hasegawa<sup>a</sup>,  
Yuka Hasegawa<sup>a</sup>, Kazuko Yonemori<sup>a</sup>, Akito Hata<sup>a</sup>, Kazunobu Aoyama<sup>a</sup> and Douglas R. Cary<sup>a,†</sup>

<sup>a</sup> *Pharmaceutical Research Division, Takeda Pharmaceutical Co., Ltd., Shonan Research Center, 26-1, Muraoka-Higashi 2-Chome,*

*Fujisawa, Kanagawa 251-8555, Japan*

<sup>b</sup> *Product Information Group Japan Oncology Business Unit, Takeda Pharmaceutical Co., Ltd., 12-10, Nihonbashi 2-Chome, Chuo-ku,*

*Tokyo 103-8686, Japan*

\* Corresponding author. Tel.: +81 466 32 1086; fax: +81 466 29 4448.

E-mail address: jun.fujimoto@takeda.com (J.Fujimoto)

† Present address: *Peptidream Inc.*

### Abstract

In this article, synthetic studies around a pyridylacrylamide-based hit compound (**1**), utilizing structure-based drug design guided by CDK8 docking models, is discussed. Modification of the pendant 4-fluorophenyl group to various heteroaromatic rings was conducted aiming an interaction with the proximal amino acids, and then replacement of the morpholine ring was targeted for decreasing potential of time-dependent CYP3A4 inhibition. These efforts led to the compound **4k**, with enhanced CDK8 inhibitory activity and no apparent potential for time-dependent CYP3A4 inhibition (CDK8 IC<sub>50</sub>: 2.5 nM; CYP3A4 TDI: 99% compound remaining). Compound **4k** was found to possess a highly selective kinase inhibition profile, and also showed favorable pharmacokinetic profile. Oral administration of **4k** (15 mg/kg, bid. for 2 weeks) suppressed tumor growth (T/C 29%) in an RPMI8226 mouse xenograft model.

### Keywords

CDK8, CDK19, Cyclin-dependent kinases (CDKs), transcriptional regulation, STAT1, MCM3, RPMI8226, SW480, DMG, pyridylacrylamide

## 1. Introduction

Cyclin-dependent kinase 8 (CDK8) belongs to the cyclin-dependent family of protein kinases and is recently highlighted as oncogene, which forms mediator complex with such as MED12 and MED13.<sup>1</sup> The mediator complex phosphorylates C-terminal domain of RNA polymerase (RNAP) II and transcriptional factors, which regulates oncogene and tumor suppressor transcription.<sup>2</sup> Other reports have shown that CDK8 plays roles in modulation of the transcription factors including Wnt/ $\beta$ -catenin pathway, Notch and TGF- $\beta$ ,<sup>3</sup> which supported the cancer-relevant activities of CDK8. In addition, copy number gain and high expression of CDK8 are observed in 60% of CRC tumors which correlates with poor prognosis of colorectal cancer patients.<sup>4</sup> CDK19 is a close homologue of CDK8 and its biological function and impact are ill defined.<sup>1b</sup>

Inhibition of CDK8 kinase activity disrupts transcription, resulting in context dependent cellular stress.<sup>5</sup> So far, several groups have disclosed CDK8 and CDK19 dual inhibitors,<sup>6</sup> which includes cortistatin derivatives,<sup>7</sup> SNX-2 class compounds,<sup>8</sup> 3,4,5-trisubstitutedpyridines,<sup>9</sup> thienopyridine analogues<sup>10</sup> and benzylindazole series.<sup>11</sup> Although the research around CDK8 is hot topic, only few selective inhibitors have been discovered.

Herein we describe our efforts to discover and optimize a series of novel and selective CDK8/19 inhibitors.<sup>12</sup> Among several classes of hits identified through a high-throughput screening (HTS) campaign, 4-phenylpyridine compound **1** (Figure 1)<sup>13</sup> was judged to be an attractive starting point to initiate a medicinal chemistry program due to its potency (CDK8 IC<sub>50</sub> = 80 nM and CDK19 IC<sub>50</sub> = 100 nM), moderate rate of metabolism in liver microsomes (5.1 mL/min/mg in human and 6.7 mL/min/mg in mouse) and acceptable physicochemical properties. In addition, **1** showed good selectivity against an in-house panel of 27 kinases (less than 20% inhibition at 1  $\mu$ M), which implied intrinsic high kinase selectivity for this series. Thus **1** was selected as a starting point for further investigation. Our medicinal chemistry efforts were largely focused on the enhancement of selective enzymatic and cellular potency, in addition to the concurrent pursuit of favorable pharmacokinetic (PK) and ADME properties, including reduction of drug-drug interaction (DDI) potential.

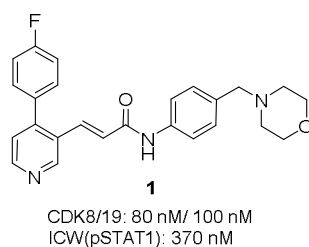


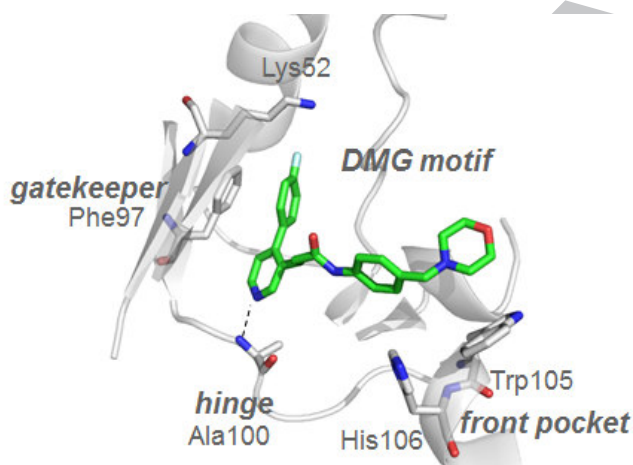
**Figure 1.** Representative hit compound identified through HTS

In the course of profiling a wide variety of HTS hits, we confirmed high correlation between the inhibitory potencies against CDK8 and CDK19, as expected based on the very high structural similarity of these two proteins (100% identity in the active site, defined as 4 Å from ligand).<sup>14</sup> Hence, during our optimization campaign we sought to enhance CDK8 inhibitory activity, with CDK19 inhibitory activity

measured as a confirmatory assay. While not discussed in detail here, CDK8 and CDK19 inhibitory potencies showed an essentially linear relation over the compounds presented in this paper, with  $IC_{50}$  ratios generally ranging from 1:1 to 1:3.<sup>9,11,12</sup>

For the identification of potent CDK8/19 inhibitors, we employed a modular structure-based drug design (SBDD) approach toward introducing modifications into our lead molecule in three separate regions. Based on a published cocrystal structure of an inhibitor bound to CDK8 (PDB ID: 3RGF)<sup>15</sup> that was obtained at the start of our investigation, a computational model of our lead **1** bound to CDK8 was constructed, as shown in Figure 2, which suggested that the central pyridine core binds to the hinge region via a hydrogen bond between the pyridine nitrogen atom and the backbone of Ala100 and this is consistent with crystallographically observed binding recently reported by other groups.<sup>9</sup> According to this model, the *p*-fluorophenyl moiety is oriented toward the back pocket region of CDK8, and the proximal Lys52, Glu66 and Asp173 of the DMG motif of CDK8 seemed attractive targets for forming additional hydrogen bonds with this molecule (Figure 2A). We therefore designed new substructures in this region as illustrated by compounds of type **2** (Figure 2B) where the *p*-fluorophenyl ring is replaced with monocyclic or fused bicyclic heterocycles with potential hydrogen

A)



B)

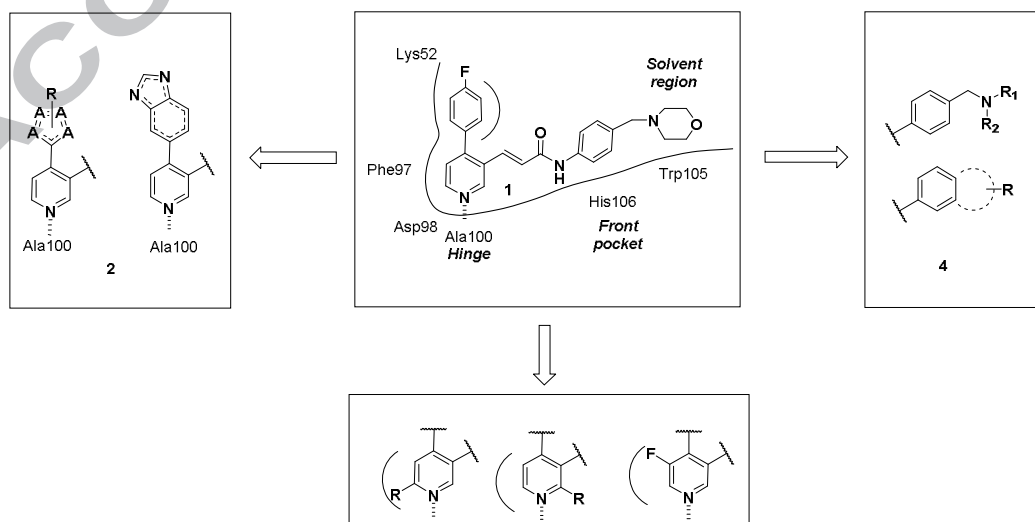


**Figure 2.** (A) Docking model of **1** (green) bound to CDK8, based on the reported structure (PDB ID, 3RGF). Key amino acid residues are depicted as sticks (gray). (B) General designs for novel CDK8/19 inhibitors.

bond acceptor and/or donor functionalities. Along a different vector, substitution of the hinge-binding pyridine was conducted with a goal of enhancing potency (generally illustrated by compounds of type **3** in Figure 2B). As with many reported kinase inhibitors, the possibility of forming hydrogen bonds at two points in the kinase hinge region was explored. From our docking studies, the backbone carbonyl oxygens of Asp98 and Ala100 were predicted to sit in close proximity to the 6- and 2-positions of the pyridine ring, respectively. Thus substituents with potential hydrogen bonding donor ability were introduced at these sites. An additional modification to the hinge binding motif was the introduction of a fluoro atom at the 5-position of the pyridine core. This design was based on the prediction of limited space around this site and the expectation of a favorable hydrophobic interaction between the fluoro atom with Ile79 and/or Phe97 in this region. The benzamide portion of **1** extends along the front of the ATP binding site and the morpholino methyl moiety is directed outward the solvent region, forming a CH- $\pi$  interaction with Trp105. Thus, this portion of the molecule was expected to allow diverse sets of substructures in terms of maintaining activity, and we modified this portion of the molecule with an aim toward improving PK and ADME properties (generally illustrated as compounds of type **4** in Figure 2B).

## 2. Chemistry

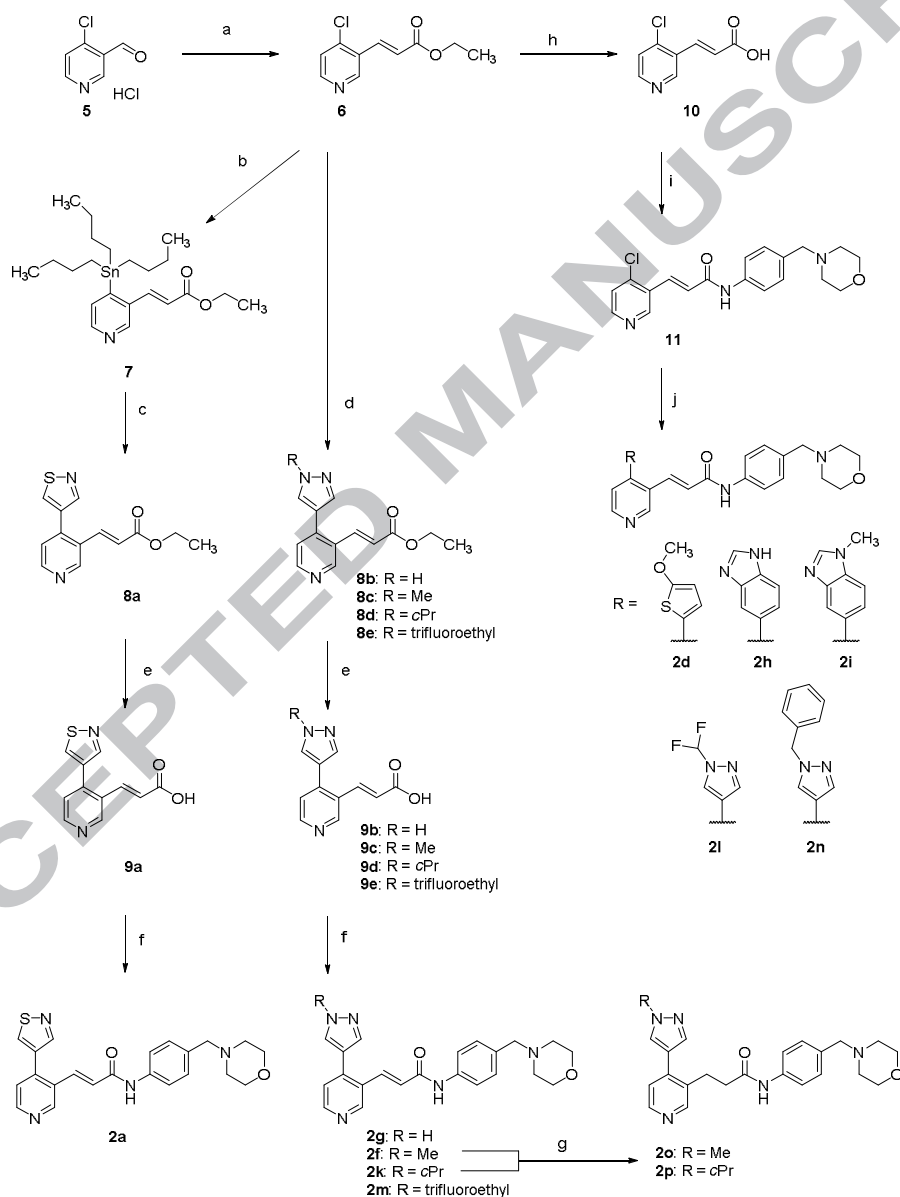
The pyridyl acrylamide derivatives reported in these studies were prepared from commercially available starting material 4-chloronicotinaldehyde hydrochloride (**5**) via the modular approach generally outlined in Scheme 1, with additional examples shown in Schemes 2–8.<sup>16</sup> The Horner-Wadsworth-Emmons reaction of **5** with triethyl phosphonoacetate afforded the desired (*E*)-alkene **6**, with minimal formation of the (*Z*)-regioisomer (<5%). Hydrolysis of **5** with sodium hydroxide provided carboxylic acid **6** in nearly quantitative yield, with these two intermediates acting as the primary starting materials for further syntheses.

Tributyltin intermediate **7** was prepared from **6** by Pd(PPh<sub>3</sub>)<sub>4</sub> mediated coupling, allowing entry into isothiazole compound **8a** by Pd(PPh<sub>3</sub>)<sub>4</sub> catalyzed coupling with 4-bromoisothiazole. Subsequent hydrolysis of **8a** to **9a** with in aqueous sodium hydroxide, followed by amide condensation with 4-(morpholinomethyl)aniline and HATU afforded isothiazole derivative **2a**.

Alternatively, palladium-mediated coupling of **6** and the appropriate boronic acids or esters using SPhos or CyJohnPhos as phosphine ligand afforded a more direct route to formation of pyrazole esters **8b–e**. Subsequent hydrolysis of the esters to their corresponding carboxylic acids with sodium hydroxide was conducted in generally good yields (71–83% for **9c–e**, 26% for highly water-soluble derivative **9b**). The preparation of amide derivatives **2g**, **2g**, **2k** and **2m** was accomplished by the reaction of 4-(morpholinomethyl)aniline and acids **9b–e**, respectively, in the presence of HATU. Reduction of the acrylamide double-bond was conducted for **2f** and **2k** to produce **2o** and **2p** by hydrogenation with Pd/C.

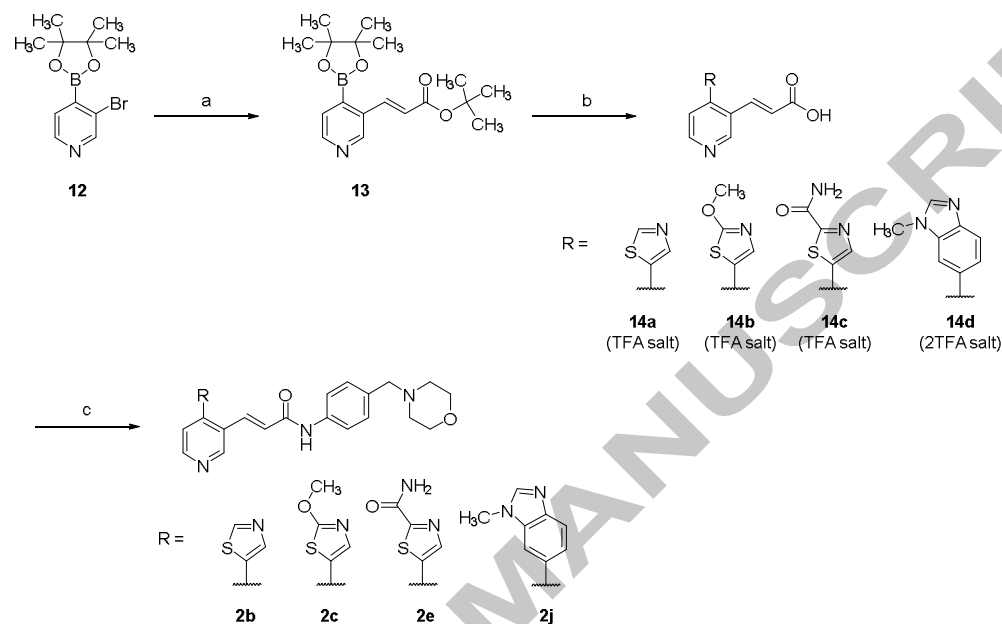
Derivatization of this modular scaffold could also be conducted in the opposite order, starting from amide bond formation between **10** and 4-(morpholinomethyl)aniline, conducted by formation of the

acid chloride of **10** with the Vilsmeier reagent, producing intermediate **11**. Key intermediate **11** was then subjected to Pd-mediated coupling, using SPhos or CyJohnPhos phosphine ligands, with the appropriate boronic acids or esters to yield **2d**, **2h**, **2i**, **2l**, and **2n**. As shown in Scheme 2, inverse coupling of aryl bromides to boronic ester based intermediate **13** was also found to be feasible. The Heck reaction of aryl bromide **12** with *tert*-butyl acrylate in the presence of Pd(OAc)<sub>2</sub> and tri-*o*-tolylphosphine afforded key boronic ester intermediate **13**. This intermediate was then subjected to palladium-catalyzed coupling with a series of heterocyclic bromides, followed by *tert*-butyl ester removal, to afford bi-aryl heterocyclic acids **14a–d**. These, in turn, were condensed with 4-(morpholinomethyl)aniline under HATU conditions to afford amide derivatives **2b**, **2c**, **2e**, and **2j**.

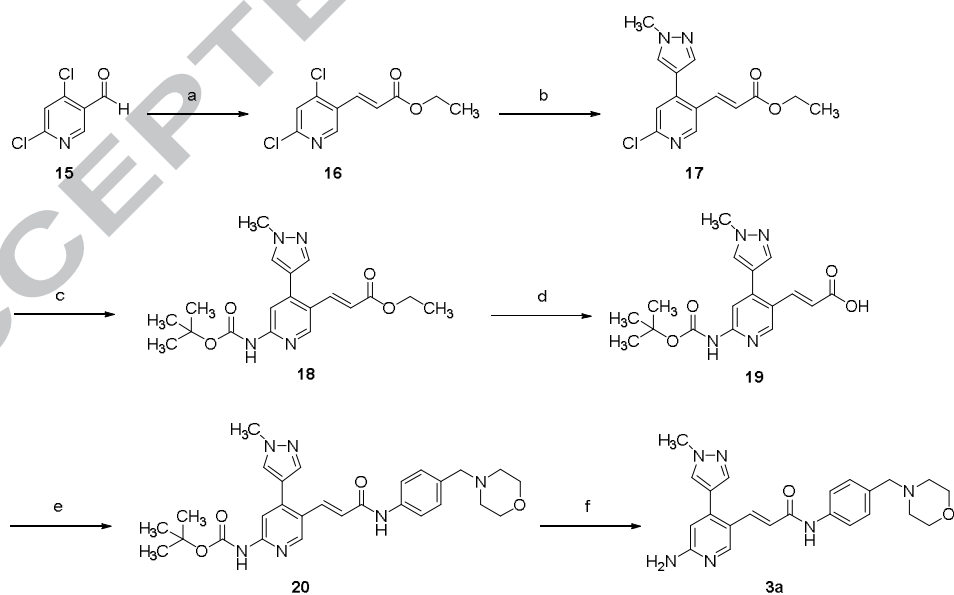


**Scheme 1.** Synthesis of **2a**, **2d**, **2f**, **2g**, **2i**, and **2k–p**. *Reagents and conditions:* (a) ethyl 2-(diethoxyphosphoryl)acetate, NaH, THF, 0 °C to rt, 86%; (b) 1,1,1,2,2,2-hexabutyldistannane, LiCl, Pd(PPh<sub>3</sub>)<sub>4</sub>, toluene, 120 °C, 19%; (c) 4-bromoisothiazole,

cesium fluoride, copper (I) iodide, Pd(PPh<sub>3</sub>)<sub>4</sub>, DMF, 100 °C, 75%; (d) boronate ester. Method A: SPhos, SPhos precatalyst 1st generation, Cs<sub>2</sub>CO<sub>3</sub>, DME, water, 130 °C, microwave irradiation, 66%. Method B: 2-(dicyclohexylphosphino)biphenyl, Pd<sub>2</sub>(dba)<sub>3</sub>, K<sub>2</sub>CO<sub>3</sub>, DME, water, 75 °C, 74–92%; (e) NaOH, water, THF, EtOH, rt, then HCl or AcOH, 26–83%; (f) 4-(morpholinomethyl)aniline, HATU, DIEA, DMF, rt, 34–83%; (g) H<sub>2</sub> (1 atm), Pd/C, EtOAc, 40 °C, 8–9%; (h) NaOH, water, THF, EtOH, rt, then aq. HCl, 96%; (i) oxalyl dichloride, DMF (5 drops), THF, rt, then 4-(morpholinomethyl)aniline, DMA, rt, 89%; (j) boronate ester or boronic acid. Method A: Cs<sub>2</sub>CO<sub>3</sub>, SPhos, SPhos precatalyst 2nd generation, DME, water, 130 °C, microwave irradiation, 43–71%. Method B: [1,1'-biphenyl]-2-ylidicyclohexylphosphine, Pd<sub>2</sub>(dba)<sub>3</sub>, Cs<sub>2</sub>CO<sub>3</sub>, DME, water, 80 °C, 45%.



**Scheme 2.** Synthesis of **2b**, **2c**, **2e** and **2j**. *Reagents and conditions:* (a) *tert*-butyl acrylate, TEA, tri-*o*-tolylphosphine, Pd(OAc)<sub>2</sub>, DMF, 130 °C, 67%; (b) (i) ArBr, Cs<sub>2</sub>CO<sub>3</sub>, SPhos, SPhos precatalyst 2nd generation, DME, water, 130 °C, microwave irradiation, (ii) TFA, rt, 34–95% in 2 steps; (c) 4-(morpholinomethyl)aniline, HATU, DIEA, DMF, rt, 73–100%.

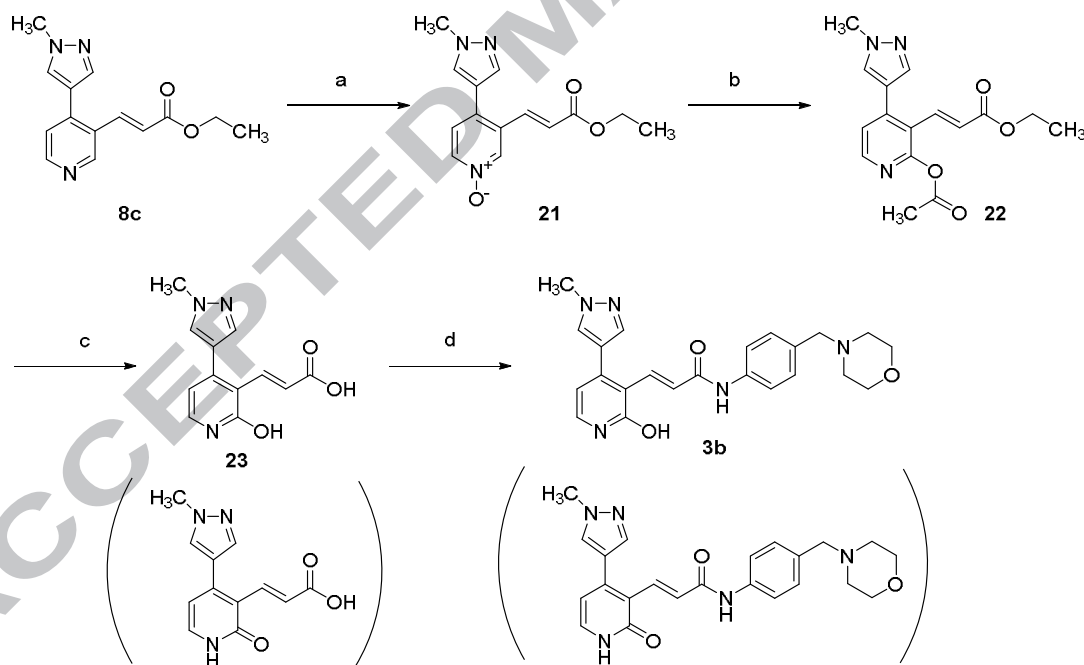


**Scheme 3.** Synthesis of **3a**. *Reagents and conditions:* (a) ethyl 2-(diethoxyphosphoryl)acetate, NaH, THF, DMF, 0 °C to rt, 98%; (b) 1-methyl-4-(4,4,5,5-tetramethyl-1,3,2-dioxaborolan-2-yl)-1H-pyrazole, [1,1'-biphenyl]-2-ylidicyclohexylphosphine, Pd<sub>2</sub>(dba)<sub>3</sub>, Cs<sub>2</sub>CO<sub>3</sub>, DME, water, 80 °C, 63%; (c) *tert*-butyl carbamate, XPhos, Pd<sub>2</sub>(dba)<sub>3</sub>, Cs<sub>2</sub>CO<sub>3</sub>, THF, 70 °C; (d) NaOH,

water, THF, EtOH, rt, then 2 M HCl, 53% in 2 steps; (e) 4-(morpholinomethyl)aniline, HATU, DIEA, DMF, rt; (f) 2 M HCl, MeOH, 45 °C, 34% in 2 steps.

Compound **3a**, an amino-substituted analogue of **2f**, was prepared by the synthetic sequence outlined in Scheme 3. Aldehyde **15** was converted to acrylic ester **16** by Horner-Wadsworth-Emmons conditions. Coupling of **16** with the appropriate N-methylpyrazole boronate ester under Pd<sub>2</sub>(dba)<sub>3</sub>/CyJohnPhos mediated conditions afforded chloropyridine intermediate **17**. The chloro group was substituted with *tert*-butyl carbamate by Pd<sub>2</sub>(dba)<sub>3</sub>/XPhos mediated coupling to afford **18**, followed by ester hydrolysis to carboxylic acid **19**. Amide condensation under HATU conditions with 4-(morpholinomethyl)aniline yielded **20**, followed by removal of the Boc-protecting group with HCl lead to the desired compound **3a**.

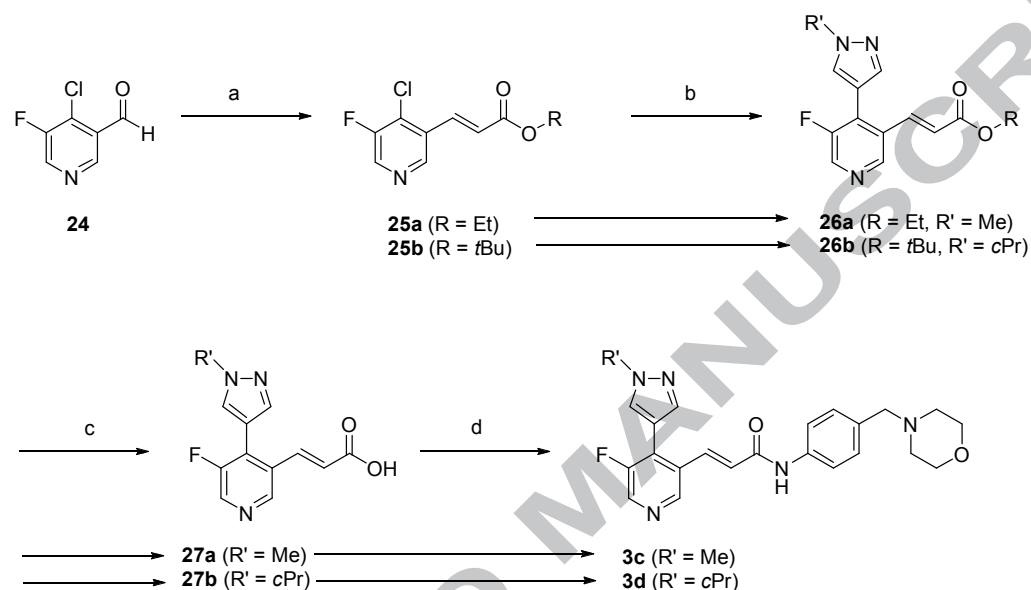
Hydroxypyridyl derivative **3b**, perhaps better described as the pyridone tautomer, was prepared according to the route shown in Scheme 4. Pyridine *N*-oxide compound **21** was prepared from **8c** and mCPBA, followed by conversion to acetyl-protected hydroxypyridine compound **22**<sup>17</sup> by heating in acetic anhydride. One-step hydrolysis of both the ethyl ester and acetate group of **22** with NaOH, followed by condensation of the resulting acid **23** with 4-(morpholinomethyl)aniline in the presence of HATU afforded the desired hydroxypyridyl compound **3b**.



**Scheme 4.** Synthesis of **3b**. Reagents and conditions: (a) mCPBA, EtOAc, rt, 66%; (b) acetic anhydride, EtOAc, 120 °C, 43%; (c) 2 M NaOH, THF, EtOH, rt; (d) 4-(morpholinomethyl)aniline, HATU, DIEA, DMF, rt, 20% in 2 steps.

In a procedure analogous to that outlined in Scheme 1, Scheme 5 shows the synthetic route used to prepare fluoropyridyl derivatives **3c** and **3d**. Starting material 4-chloro-5-fluoronicotinaldehyde (**24**) was reacted with ethyl 2-(diethoxyphosphoryl)acetate or *tert*-butyl 2-(diethoxyphosphoryl)acetate under Horner-Wadsworth-Emmons conditions to provide compounds **25a** and **25b**, respectively. Coupling with

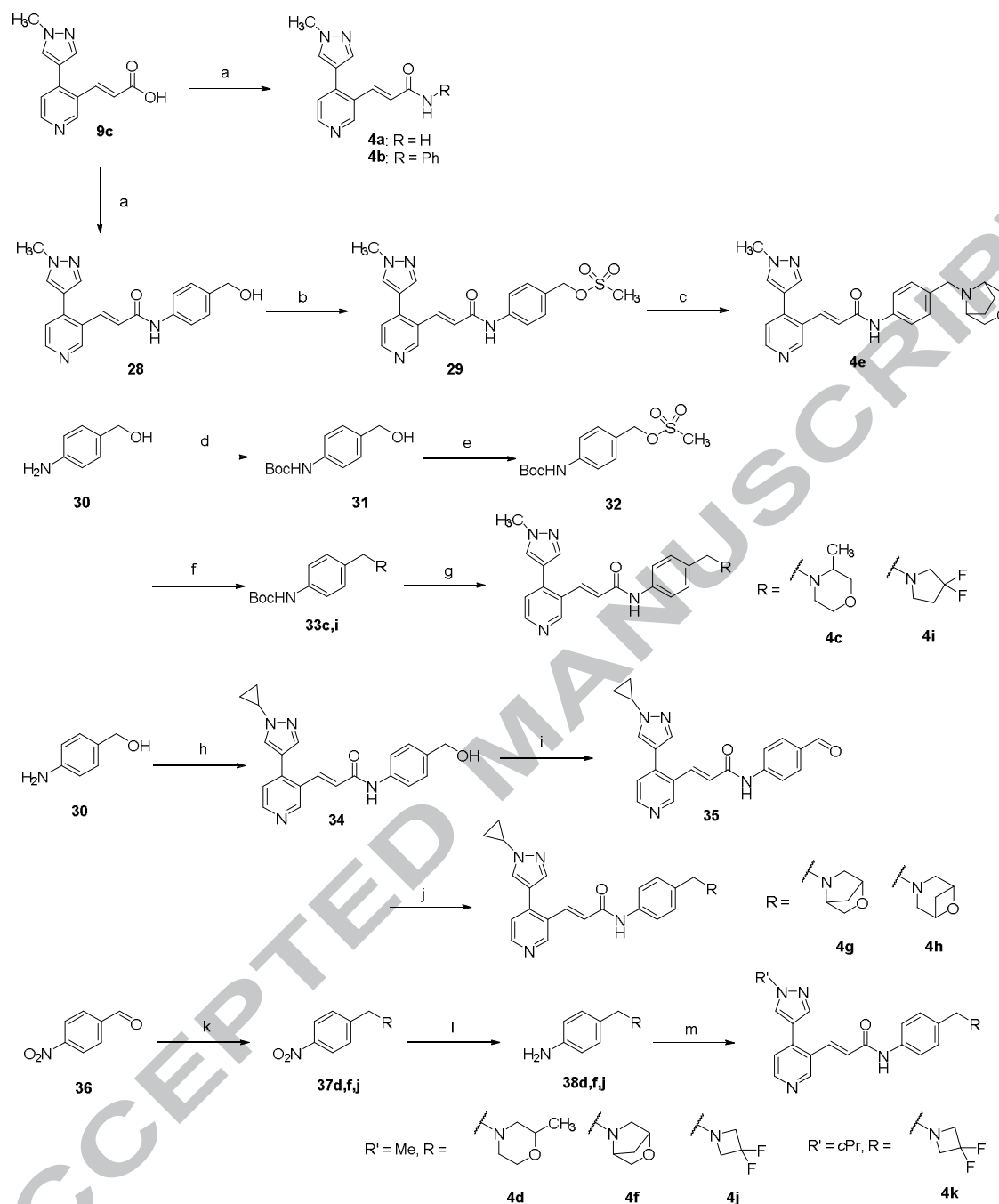
the appropriate pyrazole boronate esters in the presence of  $\text{Pd}_2(\text{dba})_3/\text{CyJohnPhos}$  catalysis afforded ester intermediates **26a** and **26b**. Methyl ester **26a** was converted to the corresponding carboxylic acid **27a** by hydrolysis with NaOH, while *tert*-butyl ester **26b** was treated with TFA and neutralized to obtain carboxylic acid **27b**. Acids **27a** and **27b** were condensed with 4-(morpholinomethyl)aniline in the presence of HATU to afford amide compounds **3c** and **3d**.



**Scheme 5.** Synthesis of **3c** and **3d**. *Reagents and conditions:* (a) for **25a**: ethyl 2-(diethoxyphosphoryl)acetate, NaH, THF, DMF, 0 °C to rt, 90%; for **25b**: *tert*-butyl 2-(diethoxyphosphoryl)acetate, NaH, THF, 0 °C to rt, 77%; (b) boronate ester, [1,1'-biphenyl]-2-yl dicyclohexylphosphine,  $\text{Pd}_2(\text{dba})_3$ ,  $\text{Cs}_2\text{CO}_3$ , DME, water, 85 °C, 75–82%; (c) for **27a**: 2 M NaOH, THF, EtOH, 0 °C to rt, 60%; for **27b**: TFA, then 2 M NaOH, 0 °C to rt, 93%; (d) 4-(morpholinomethyl)aniline, HATU, DIEA, DMF, rt, 69–72%.

Modifications at the morpholine moiety were conducted by the routes shown in Scheme 6. Compounds **4a**, **4b**, and **28** were prepared by amide coupling of **9c** and the appropriate amines. The mesylate of **28** was prepared, compound **29**, and subjected to nucleophilic substitution with the appropriate bicyclic morpholine derivative to yield **4e**. In a related approach, Boc-protected anilines **33c** and **33i** were prepared from amino alcohol **30** by a similar sequence of Boc protection to give **31**, followed by mesylation of the benzylic alcohol to afford **32**, and finally nucleophilic substitution with the appropriate amines to provide the desired intermediates **33c** and **33i**. Boc-deprotection followed by amide condensation with **9c** to yield products **4c** and **4i**.

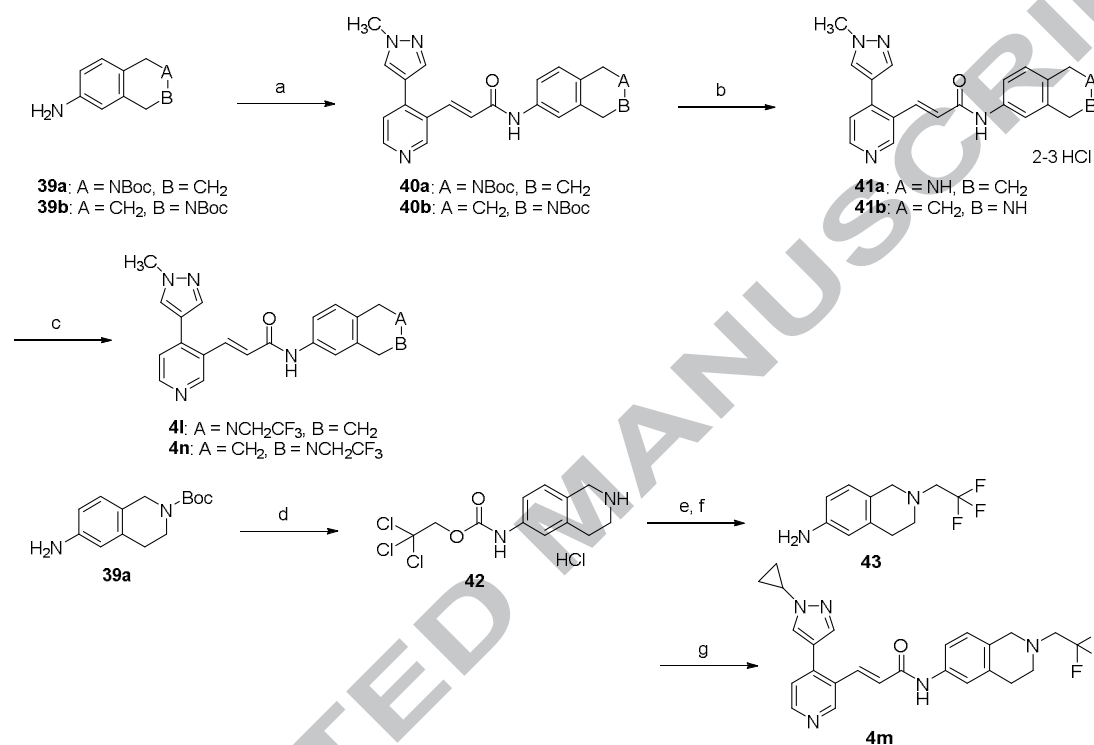
Reductive amination routes to related derivatives were also utilized. Cyclopropyl compound **34** was prepared analogously to compound **28**, followed by  $\text{MnO}_2$  oxidation of the benzylic alcohol to yield aldehyde **35**. Reductive amination with the appropriate amines in the presence of 2-picolone borane complex afforded compounds **4g** and **4h**. Alternatively, initial synthesis of aniline intermediates **38d**,



**Scheme 6.** Synthesis of **4a–4k**. *Reagents and conditions:* (a) R-NH<sub>2</sub>, HOBt, EDCl, DMF, rt, or R-NH<sub>2</sub>, HATU, DIEA, DMF, rt, 34–99%; (b) MsCl, NEt<sub>3</sub>, CH<sub>2</sub>Cl<sub>2</sub>, 0 °C to rt; (c) amine hydrochloride, NaH, DMF, rt, 4% in 2 steps; (d) Boc<sub>2</sub>O, DIEA, THF, reflux, 59%; (e) MsCl, NEt<sub>3</sub>, CH<sub>2</sub>Cl<sub>2</sub>, rt, 68%; (f) amine hydrochloride, NaH, DMF, rt, 19–21%; (g) (i) HCl, EtOH, rt; (ii) **9c**, HATU, DIEA, DMF, rt, 16–22%; (h) **9d**, HATU, DIEA, DMF, rt, 69%; (i) MnO<sub>2</sub>, THF, 63%; (j) amine hydrochloride, 2-picolone borane complex, MeOH, AcOH, 19–41%; (k) amine hydrochloride, dichloroethane, rt, then NaBH(OAc)<sub>3</sub>, rt, 27–54%; (l) Fe, NH<sub>4</sub>Cl, EtOH, water, 70 °C, 62–80%; (m) **9c** or **9d**, HATU, DIEA, DMF, rt, 13–57%.

**38f**, and **38j** could be accomplished by reductive amination of aldehyde **36**, followed by reduction of the nitro group of compounds **37d**, **37f**, and **37j**. These anilines could then be condensed with **9c** or **9d** in the presence of HATU to yield amide derivatives **4d**, **4f**, **4j**, and **4k**.

Tetrahydroisoquinoline-based derivatives **41–4n** were prepared as shown in Scheme 7. Amide condensation of amines **39a** or **39b** with **9c** under HATU conditions afforded amine compounds **40a** and **40b**, which we then subjected to standard Boc-deprotection and alkylation to afford trifluoroethyl compounds **41** and **4n**, respectively. Alternatively, 2,2,2-trichloroethyl carbamate (Troc) protection and Boc-removal from **39a**, followed by alkylation of **42**, afforded aniline intermediate **43**. This compound was then condensed with **9d** under HATU conditions to afford **4m**.



**Scheme 7.** Synthesis of **41–4n**. *Reagents and conditions:* (a) **9c**, HATU, DIEA, DMF, rt, 76–95%; (b) HCl, EtOAc or CPME, MeOH, 86%; (c) NEt<sub>3</sub>, TfOCH<sub>2</sub>CF<sub>3</sub>, CH<sub>3</sub>CN, rt to 50 °C, 32–51%; (d) TrocCl, NEt<sub>3</sub>, THF then HCl/EtOAc, 90%; (e) TfOCH<sub>2</sub>CF<sub>3</sub>, NEt<sub>3</sub>, DMF; (f) Zn, AcOH, 69% in 2 steps; (g) **9d**, HATU, DIEA, DMF, 65%.

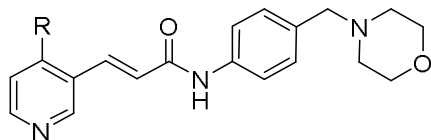
### 3. Results and discussion

CDK8 and CDK19 binding activities of the newly synthesized compounds were evaluated by kinase tracer assay, in which inhibition of binding of kinase tracer 236 to CDK8 or CDK19 was detected by fluorescence measurement. Cellular activity of our compounds was evaluated by an in-cell western (ICW) assay, in which each compound was incubated with SW480 cells (human colorectal adenocarcinoma) fixed on a plate, and the inhibition of Ser727 phosphorylation of STAT1 (a direct substrate of CDK8<sup>18</sup>) following IFN- $\gamma$  stimulation was measured. In vitro activities measured in the above assay types are reported as IC<sub>50</sub> and EC<sub>50</sub> values, respectively.

The effect of replacement of the *p*-fluorophenyl moiety with various heterocycles is illustrated in Table 1. According to the strategy described in the Introduction, a variety of heterocyclic derivatives were prepared, with a particular focus on 5-membered heterocycles (**2a–g**) and benzimidazoles (**2h–j**). First, 4-isothiazoyl and 5-thiazoyl analogues (**2a** and **2b**) were prepared, which showed 2–3 times more

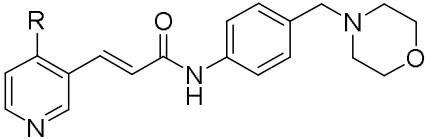
potent CDK8 binding activities than **1**. The next approach taken was the introduction of a substituent containing a hydrogen bonding acceptor into the 5-membered rings (**2c–e**). Of particular interest was the finding that 2-methoxythiazole **2c** and 2-aminocarboxythiophene **2e** displayed more than a 9-fold increase in binding activity compared to **1**, which supported our aim to target Lys52, Glu66 and/or Asp173 as a hydrogen bonding partner. The difference in potency between **2c** and **2d** may be derived from the thiazole nitrogen atom restricting the direction and donor ability of the methoxy oxygen lone pair to interact with the protein. Encouraged by these results, derivatives containing other 5-membered heterocycles (pyrazoles **2f** and **2g**) were prepared. The binding potency of 1-methyl pyrazole **2f** was found to be 12-fold higher than **1**, and 1-H pyrazole **2g** exhibited a further 12-fold increase in binding potency, with an IC<sub>50</sub> value of less than 1 nM. Although our docking study suggested that these pyrazole moieties would not be expected to form a direct hydrogen bonding interaction with Lys52, Glu66 or Asp173, it is thought that they could interact via a water molecule. The increased activity observed for compounds **2f** and **2g** was also reflected in the cellular assays; both compounds exhibited more than 17-fold greater potency in the ICW assay relative to **1**. The preparation of benzimidazoles (**2h–j**) was a further attempt at targeting interaction with Lys52, Glu66 and/or Asp173, with **2h** and **2j** showing high potency in both the biochemical and cellular assays. These results supported the validity of our drug design strategy, however, further study of this compound class was discontinued due to the generally potent hERG inhibitory activity (data not shown).

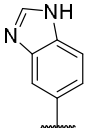
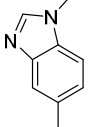
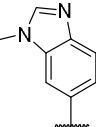
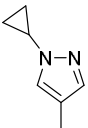
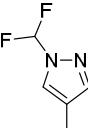
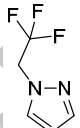
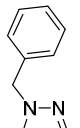
Among the most potent compounds identified above (**2c**, **2f** and **2g**), methylpyrazole derivative **2f** showed the most favorable PK profile in mouse cassette dosing studies (Table 2 includes the data for **2f**) and became the focus of further optimization efforts. In vivo metabolite analysis of **2f** in mice revealed the primary sites of metabolism to be the morpholine moiety and the 1-methyl group of the pyrazole (Figure 3). Thus, further modification of the pyrazole 1-methyl group was conducted with a goal of improving metabolic stability and PK, while maintaining enzymatic potency. The approaches taken in these studies were 1) blockage of the metabolically unstable methyl site and 2) installation of a bulky substituent into the methyl group, leading to the preparation of compounds **2k–n** (Table 1). Generally speaking, variation of the alkyl group in this position showed limited tolerance with respect to potency, namely, cyclopropyl derivative **2k** possessed comparable activity to parent compound **2f** while other fluorinated alkyl substituents such as **2l** and **2m** showed reduced enzymatic potency. Interestingly, potency was maintained for benzyl derivative **2n**, implying that this moiety could be oriented toward the back pocket region of CDK8. Subsequent mouse cassette dosing studies demonstrated a better PK profile for cyclopropyl derivative **2k** relative to methyl pyrazole **2f**, while benzyl compound **2n** showed poor

**Table 1**Biological activities of **1** and derivatives **2a–n**

compd.	R	CDK8 <sup>a</sup>		pSTAT1 <sup>b</sup>	
		IC <sub>50</sub> (nM)		EC <sub>50</sub> (nM)	
<b>1</b>		80 (69-92)		370 (201-673)	
<b>2a</b>		27 (21-35)		110 (51-222)	
<b>2b</b>		41 (34-50)		140 (50.2-399)	
<b>2c</b>		8.1 (6.5-10.0)		12 (5.4-26)	
<b>2d</b>		28 (22-34)		97 (30-315)	
<b>2e</b>		8.3 (6.3-11.0)		690 (278-1712)	
<b>2f</b>		6.5 (5.8-7.2)		13 (10-18)	
<b>2g</b>		0.54 (0.31-0.94)		21 (14-30)	

Table 1 . (continued)



compd.	R	CDK8 <sup>a</sup>	pSTAT1 <sup>b</sup>
		IC <sub>50</sub> (nM)	EC <sub>50</sub> (nM)
2h		1.5 (1.0-2.4)	10 (5.7-18)
2i		4800 (3065-7502)	>10000
2j		2.5 (2.1-3.0)	2.4 (1.5-3.9)
2k		6.4 (5.0-8.3)	11 (4.5-26)
2l		24 (21-27)	50 (16-152)
2m		28 (23-35)	150 (78-290)
2n		4.5 (3.6-5.7)	28 (15-54)

<sup>a</sup> Inhibition of kinase tracer 236 binding to human CDK8 (n = 2, values in parentheses indicate 95% confidence interval).

<sup>b</sup> Inhibition of STAT1 phosphorylation (at Ser727) induced by IFN- $\gamma$  in SW480 cells fixed on a 384-well plate (values in parentheses indicate 95% confidence interval).

**Table 2**

PK profiles and metabolic stabilities of selected compounds

compd.	Cl <sub>total</sub> <sup>a</sup> (mL/h/kg)	C <sub>max</sub> <sup>b</sup> (ng/mL)	AUC po <sup>c</sup> (ng/mL*h)	MRT po <sup>d</sup> (h)	F <sup>e</sup> (%)	Metabolic stability <sup>f</sup> (mL/min/mg)	
						human	mouse
<b>2f</b>	2967	47.5	76.9	1.5	21.9	22	77
<b>2k</b>	1523	207.7	339.7	1.5	51.2	25	64
<b>2n</b>	5765	15.7	26.9	1.2	15.5	78	118

PK data obtained from mouse cassette dosing studies (1 mg/kg, po, 0–8 h).

<sup>a</sup> Cl<sub>total</sub>: mean plasma clearance.

<sup>b</sup> C<sub>max</sub>: maximum concentration.

<sup>c</sup> AUC<sub>po</sub>: area under the curve.

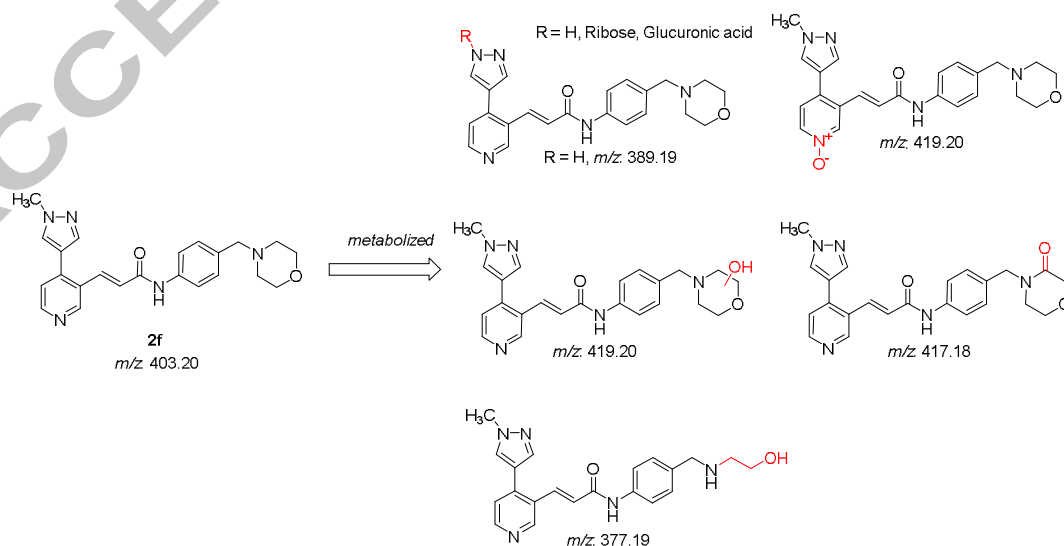
<sup>d</sup> MRT<sub>po</sub>: mean residence time.

<sup>e</sup> F: bioavailability in mouse cassette dosing studies (0.1 mg/kg, iv and 1 mg/kg, po).

<sup>f</sup> Metabolic stability in human or mouse hepatic microsomes.

metabolic stability in mouse microsomes. Based on these results, 1-methyl and 1-cyclopropyl pyrazoles **2f** and **2k** were chosen as templates for further SAR studies in other sections of this chemistry.

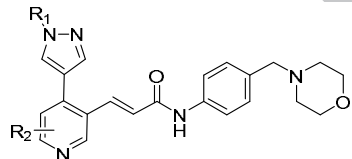
As a next focus, modifications were made to the hinge-binding pyridine core with the aim of improving potency and the resulting compounds **3a–d** are shown in Table 3. Our first design strategy was the introduction of a two-point hydrogen bond utilizing hinge residue Ala100 and proximal Asp98 (Figure 2A), which resulted in the preparation of compounds **3a** and **3b** possessing an amino or hydroxyl group adjacent to the pyridine N-position. However, the potencies of both compounds proved to be dramatically decreased compared to the parent **2f**. Subsequently, we undertook the installation of a fluoro atom at the 5-position of the pyridine core, resulting in the preparation of **3c** and **3d**. The fluoro atom was expected to sit in a small space adjacent to Ile79 and Phe97 based on our computational model (Figure 2A) and potent enzymatic activity was maintained for these compounds. In addition, the inhibitory activity of STAT1 phosphorylation (ICW assay) was increased for both compounds with respect to the corresponding non-substituted analogues (**2f** and **2k**).

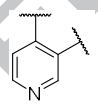
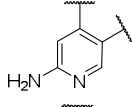
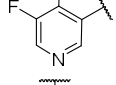
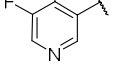


**Figure 3.** Presumed structures for metabolites of **2f** (in mouse plasma) based on MS analysis

ACCEPTED MANUSCRIPT

During the process of profiling our lead compounds **2f** and **2k**, we found that they exhibit time-dependent inhibition (TDI) of CYP3A4 in our routine in-house in vitro ADME assay (Table 3). Of particular interest was the finding that 3-fluoropyridine derivatives **3c** and **3d** showed increased TDI potential. TDI is also referred to as mechanism-based inhibition, which results from irreversible binding of the test compound itself or a reactive metabolite to CYP3A4. Inhibitory activity against CYP3A4 is considered a substantial concern in terms of drug safety, due to the potential for decreasing drug clearance and the induction of unpredictable toxicity (hepatotoxicity, idiosyncratic drug toxicity, etc.). Thus, we sought to reduce the TDI activity of our compounds during optimization. First, we postulated that the alkene linker between the hinge-binding pyridine and benzamide moiety might be responsible for TDI, but replacement of this linker with an ethylene structure showed little influence on TDI potential (Figure 4, **2o** and **2p**). In addition, these modifications substantially decreased both enzymatic and cellular activities. Thus our focus was shifted to other

**Table 3**Biological activities of **2f**, **2k** and substituted pyridine derivatives **3a–d**


compd.	R <sub>1</sub>	R <sub>2</sub>	CDK8 <sup>a</sup> IC <sub>50</sub> (nM)	pSTAT1 <sup>b</sup> EC <sub>50</sub> (nM)	CYP3A4 TDI <sup>c</sup> (% remaining @ 30 μM)
<b>2f</b>	Me		6.5 (5.8-7.2)	13 (9.6-18)	81
<b>2k</b>	<i>c</i> Pr		6.4 (5.0-8.3)	11 (4.5-25)	54
<b>3a</b>	Me		990 (787-1248)	1300 (392-4389)	ND <sup>d</sup>
<b>3b</b>	Me		> 10000	> 10000	89
<b>3c</b>	Me		5.2 (4.5-5.9)	3.6 (2.3-5.5)	60
<b>3d</b>	<i>c</i> Pr		6.5 (5.7-7.5)	2.3 (0.95-5.3)	46

<sup>a</sup> Inhibition of kinase tracer 236 binding to human CDK8 (n = 2, values in parentheses indicate 95% confidence interval).

<sup>b</sup> Inhibition of STAT1 phosphorylation (at Ser727) induced by IFN- $\gamma$  in SW480 cells fixed on a 384-well plate (values in parentheses indicate 95% confidence interval).

<sup>c</sup> % remaining of CYP3A4 activity. Tested compounds were pre-incubated in human liver microsomes for 60 min.

Testosterone was added to microsomes and incubated for 20 min.

<sup>d</sup> ND: not determined.

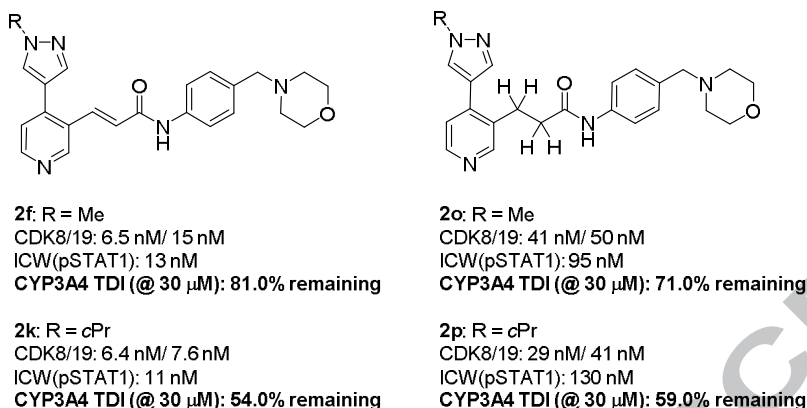


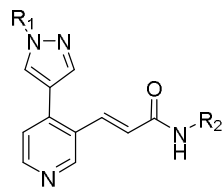
**Figure 4.** Effects on biological activity and TDI potential upon modification of the alkene linker.

sections of the molecule, especially the right-hand region of this series. As illustrated in Figure 4, one of the more metabolically labile portions of these compounds was found to be the morpholine moiety, and we postulated that the morpholine group could be converted to a reactive imine species during the metabolic process based on metabolite identification studies using LCMS. Therefore, we prepared derivatives in which the morpholine moiety was replaced with other basic amines, such as those shown in Table 4. Initially, we prepared compounds **4a** and **4b**, which demonstrated the importance of the benzamide phenyl ring for potent CDK8 binding activity. Compared to **2f**, the enzymatic potency of **4b** was reduced by more than a 7-fold and the morpholinomethyl moiety was also found to be important for potent activity. In addition, the solubility of **4b** in pH6.8 was inferior to **2f**, which showed that this morpholine was a key to address good physicochemical property of the compound. While not discussed here in detail, the phenyl ring was predicted to be close to His106 and important for high binding affinity via a CH- $\pi$  interaction based on our computational model, and replacement with aliphatic or heteroaromatic rings was found to result in significantly reduced enzymatic potency (See Supplementary Figure 2). In terms of CYP3A4 TDI potential, compound **4b** was found to show low risk, which supported our assumption that the morpholine was playing a major role in the TDI potential for this chemical series. Thus, substituted morpholine analogues **4c** and **4d**, which were expected to be more metabolically stable, were synthesized but showed no advantage over **2f** in terms of activity or CYP3A4 inactivation. An important clue regarding the origin of the observed TDI effect was obtained from the preparation and study of bicyclic morpholine derivatives **4e-h**. A previous report from Genentech on mTOR inhibitors suggested that a bicyclic tropane system could be employed to prevent reactive metabolite formation due to the high strain energy of the resulting iminium bridgehead double bond (Bredt's rule).<sup>19</sup> Notably, our bicyclic morpholine compounds showed dramatically improved TDI profiles, with compounds **4f** and **4g** showing comparable in vitro activity to **2f** and **2k**. Although both compounds show somewhat less favorable PK profiles than **2l** (data not shown), these derivatives encouraged us to further investigate pyrrolidine and azetidine derivatives **4i-k** as simplified morpholine analogues with increased ring strain. While **4i** did not

display reduced CYP3A4 TDI potential, azetidines **4j** and **4k** showed almost complete elimination of TDI risk. We postulate that inclusion of the azetidine ring reduces TDI of CYP3A4 by virtue of the conformationally restricted 4-membered ring prohibiting double-bond iminium formation. Moreover, compound **4k** showed high potency in both the biochemical and cellular assays, and sufficient level of solubility in pH6.8. Compounds **4l-n** represent further modifications of the right-hand region. Preparation of these saturated fused ring systems aimed to remove the morpholine structure and gain more effective CH- $\pi$  interaction with Trp105. Tetrahydroisoquinoline replacement (**4l-n**) resulted in high enzymatic and cellular potency with moderate to strong CYP3A4 TDI potential.

**Table 4**

Biological activities of **2f**, **2k** and derivatives **4a-n**



compd.	R <sub>1</sub>	R <sub>2</sub>	CDK8 <sup>a</sup> IC <sub>50</sub> (nM)	pSTAT1 <sup>b</sup> EC <sub>50</sub> (nM)	CYP3A4 TDI <sup>c</sup> (% remaining @ 30 μM)	Solubility <sup>e</sup> pH6.8 (μg/mL)
2f	Me		6.5 (5.8-7.2)	13 (10-18)	81	68
2l	<i>c</i> Pr		6.4 (5.0-8.3)	11 (4.5-25)	54	58
4a	Me	H	> 10000	> 10000	ND <sup>d</sup>	ND <sup>d</sup>
4b	Me	Ph	51 (43-61)	110 (52.1-237)	97	26
4c	Me		20 (14-28)	27 (16-47)	59	>75
4d	Me		6.7 (4.8-9.4)	16 (12-22)	84	ND <sup>d</sup>
4e	Me		6.3 (4.3-9.3)	17 (10-29)	99	ND <sup>d</sup>
4f	Me		16 (13-20)	19 (12-29)	100	>82
4g	<i>c</i> Pr		9.6 (8.8-10.6)	3.1 (1.2-7.9)	101	>92
4h	<i>c</i> Pr		6.7 (5.0-9.0)	5.5 (2.1-14.4)	108	60

Table 4. (continued)

compd.	R <sub>1</sub>	R <sub>2</sub>	CDK8 <sup>a</sup>	pSTAT1 <sup>b</sup>	CYP3A4 TDI <sup>c</sup>	Solubility <sup>e</sup>
			IC <sub>50</sub> (nM)	EC <sub>50</sub> (nM)	(% remaining @ 30 μM)	pH6.8 (μg/mL)
<b>4i</b>	Me		6.2 (5.1-7.5)	17 (11-25)	69	33
<b>4j</b>	Me		11 (8.6-13)	84 (27-262)	98	44
<b>4k</b>	<i>c</i> Pr		2.5 (2.2-2.8)	8.4 (6.1-11.5)	99	30
<b>4l</b>	Me		4.5 (3.0-6.8)	7.0 (4.8-10.2)	91	>81
<b>4m</b>	<i>c</i> Pr		7.1 (5.5-9.1)	14 (7.8-24.6)	88	3.9
<b>4n</b>	Me		3.2 (2.6-4.1)	8.4 (5.1-14.0)	22	8.9

<sup>a</sup> Inhibition of kinase tracer 236 binding to human CDK8 (n = 2, values in parentheses indicate 95% confidence interval).

<sup>b</sup> Inhibition of STAT1 phosphorylation (at Ser727) induced by IFN- $\gamma$  in SW480 cells fixed on a 384-well plate (values in parentheses indicate 95% confidence interval).

<sup>c</sup> % remaining of CYP3A4 activity. Tested compounds were pre-incubated in human liver microsomes for 60 min. Testosterone was added to microsomes and incubated for 20 min.

<sup>d</sup> ND: not determined.

**Kinase selectivity of 4k.** As a representative of our CDK8/19 inhibitors, compound **4k** (inhibitory potency: CDK8 IC<sub>50</sub> = 1.3 nM, CDK19 IC<sub>50</sub> = 3.9 nM) was screened against a panel of 456 kinases in a binding assay to determine its selectivity (KINOMEscan<sup>TM</sup> from DiscoverX Corp.).<sup>20</sup> At a concentration of 300 nM, compound **4k** did not bind to any of the 456 kinases tested with >65% binding affinity (<35% control), except CDK8 and CDK19 (Supplementary Figure 1). This high level of selectivity is believed due to a combination of the effective interaction of **4k** with several amino acid residues characteristic for CDK8. For instance, according to our docking studies, gatekeeper Phe97 and the unusual DMG motif of the CDK8 protein are located in proximity to the inhibitor (Supplementary Figure 2A). Analysis of kinase sequences<sup>3</sup> showed that these features are characteristic of CDK8 and interaction with these residues would differentiate it from other kinases (Supplementary Figure 2B).

**In vitro pharmacology of 4k.** According to the results discussed above, we focused further studies on azetidine compound **4k**, which showed potent in vitro activity and virtually no CYP3A4 TDI. Table 5 shows the results of Western blotting and cell proliferation for three representative cell lines: SW480 (colon cancer), RPMI8226 (human myeloma) and EOL1 (AML). While phosphorylation inhibition of STAT1 in SW480 cells was measured above as a primary screen of in vitro cellular activity, inhibition of cell growth in this cell line could not be suppressed below 50%; therefore, this cell line was not utilized for measurement of cell growth inhibition. Compound **4k** suppressed phosphorylated-STAT1 levels in all cell lines tested, and also demonstrated potent anti-proliferative activity against RPMI8226 ( $GI_{50}$ : 21.0 nM) and EOL1 ( $GI_{50}$ : 6.5 nM). Based on these results, we have found that phospho-STAT1 is a target engagement marker, which is suppressed by **4k** in these and other cell lines, but does not always reflect the sensitivity of cell growth. Other predictive markers for cell growth inhibition are under investigation and will be published in due course.

**Table 5**

STAT1 suppression after 1 day treatment with **4k** (Western blotting: WB) in various cell lines, and the corresponding anti-proliferative activity ( $GI_{50}$ ).

Cell line	Organ	WB: Phospho-STAT1			Cell Proliferation <sup>a</sup> $GI_{50}$ (nM)
		0	3	30 (nM)	
SW480	Colon	pS727-STAT1			
		STAT1			
		$\beta$ -actin			
RPMI8226	Multiple Myeloma	pS727-STAT1			
		STAT1			
		$\beta$ -actin			
EOL1	AML	pS727-STAT1			
		STAT1			
		GAPDH			

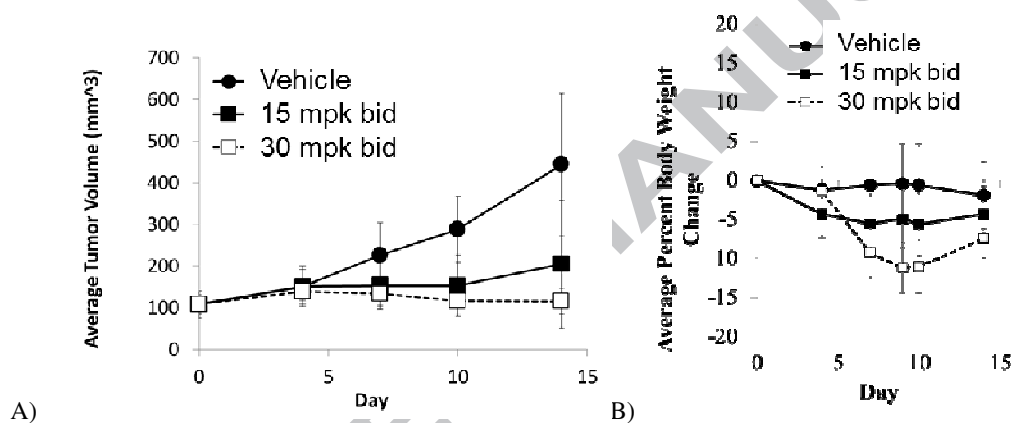
<sup>a</sup> Cell proliferation was determined by ATP content (SW480 and RPMI8226) or by nuclear count (EOL1). Cells were exposed to a compound for 168 h.

**In vivo pharmacology of 4k.** The favorable PK profile of **4k** in mice and high metabolic stability against human microsomes (Table 6) lead us to consider this compound as a promising candidate for further pharmacological evaluation.

Antitumor efficacy studies were conducted using compound **4k** in order to demonstrate the effects of CDK8/19 inhibition on tumor growth in mice. Compound **4k** was administered orally twice a day at 15 and 30 mg/kg for 2 weeks to mice bearing RPMI8226 tumor xenografts. Tumor growth was measured over the course of the study and is presented in Figure 5A. When compared to vehicle control, compound **4k** demonstrated 29% and -2% T/C values (ratio of tumor volume for treatment group vs. control) at doses of 15 and 30 mg/kg, respectively. Furthermore, compound **4k** was well tolerated with no severe changes in body weight at a dose of 15 mg/kg while 12% loss of body weight was observed in 30 mg/kg dosing (Figure 5B). On the last day of the studies, mouse blood was sampled at timepoints of 2 h and 8 h post-dose, and inhibition of phosphorylation of STAT1 was measured as a PD marker. Compound **4k** demonstrated a decrease in production of phosphorylated-STAT1 at each time point (Supplementary Figure 3), indicating in vivo inhibition of CDK8 by our novel compound.

**Table 6**Growth inhibitory activity, PK profile in mouse, and metabolic stability of compound **4k**

compd.	Cell Growth <sup>a</sup> GI <sub>50</sub> (nM)	C <sub>max</sub> <sup>b</sup> (ng/mL)	AUC po <sup>c</sup> (ng/mL*h)	MRT po <sup>d</sup> (h)	F <sup>e</sup> (%)	Metabolic stability <sup>f</sup> (mL/min/mg)	
						human	mouse
<b>4k</b>	21	321	370	1.6	22.5	15	97

<sup>a</sup> Inhibition of RPMI8226 tumor cell growth.<sup>b</sup> C<sub>max</sub>: maximum concentration (1 mg/kg, po, 0–8h).<sup>c</sup> AUC<sub>po</sub>: area under the curve (1 mg/kg, po, 0–8h).<sup>d</sup> MRT<sub>po</sub>: mean residence time in a discrete study (1 mg/kg, po, 0–8h).<sup>e</sup> F: bioavailability (1 mg/kg, po, 0–8h).<sup>f</sup> Metabolic stability in human or mouse hepatic microsomes.**Figure 5.** (A) Antitumor activity and (B) body weight loss of **4k** in a RPMI8226 mouse xenograft model.

#### 4. Conclusion

In this paper, we report the discovery of a novel class of CDK8/19 inhibitors. Starting from HTS hit **1**, an optimization campaign was initiated with a primary goal of potency enhancement, as well as achieving favorable PK and ADME profiles. By the utilization of a computational model of compound **1** bound to CDK8, constructed from a reported co-crystal structure of ligand-bound CDK8, we efficiently optimized our lead compound using a modular structure-based approach. First, heteroaromatic rings were introduced as alternatives to the *p*-fluoro phenyl moiety, leading to the identification of 1-methyl and 1-cyclopropyl pyrazole analogues with substantially enhanced potency and favorable PK properties. In addition, the introduction of a fluoro atom into the central pyridine core maintained enzymatic activity and significant enhancement of cellular activity. Although moderate to strong risk of CYP3A4 TDI was observed in the course of working on this series, changing the pendant morpholine ring to structurally restricted ring systems (bridged morpholine or azetidine) was found to be an effective method to alleviate

this issue, which finally led to the identification of compound **4k**. This compound demonstrated anti-tumor efficacy in RPMI8226 mouse xenograft studies and excellent selectivity toward CDK8/19 inhibition against a panel of 456 kinases, which supported our expectation that inhibition of CDK8/19 holds potential as a new approach for treating cancer. According to the results discussed in this paper, compound **4k** was selected as a development candidate and progressed into toxicity studies.

## 5. Experimental section

**5.1. Docking studies.** Docking study with reported CDK8 crystal structure (PDB ID; 3RGF) was performed using GOLD version 5.2 (Cambridge Crystallographic Data Centre: CCDC).

**5.2. Ligand displacement assay against CDK8 and CDK19 kinases.** Ligand displacement assay was conducted with Tb-labeled anti-GST antibody (CisBio), 20 nM Kinase Tracer 236 (ThermoFischer), 20 nM GST-CDK8/CycC (CarnaBio) or GST-CDK19/CycC (CarnaBio), and compounds. All components were diluted in the assay buffer containing 25 mM HEPES, 10 mM MgCl<sub>2</sub>, 2 mM DTT, 0.01 % Tween-20. After 60 min incubation at rt, TR-FRET was measured on EnVision plate reader (PerkinElmer).

**5.3. In-Cell western assay of pSTAT1 in SW480 cells.** Human colon adenocarcinoma cell line, SW480, was maintained in the Leibovits L-15 medium (Gibco) with 10 % FBS at 37 °C. Cells were plated on 384 well plates at a density of 6000 cells/well. After overnight incubation, cells were treated with compounds for two hours then treated with 10 ng/mL interferon- $\gamma$  for one hour. Cells were fixed with Mildform 20 NM (wako) then washed with PBS. Cells were permeabilized and blocked with 0.1% Triton-X-100, 0.05% Porcine300, 10% goat serum in PBS at rt for one hour. After discarding the blocking buffer, cells were treated with phospho-STAT1 (Ser727) (D3B7) Rabbit mAb (Cell Signaling Technology) at 4 °C. After overnight incubation and wash with 0.1% Triton X-100 in PBS (PBS-T), secondary detection was conducted with Goat anti-Rabbit IRDye 800CW (LiCor) and DRAQ5 (Cell Signaling Technology) for one hour at rt. After five washes with PBS-T, pSTAT1 and DNA were visualized using Odyssey Infrared Imaging Scanner (LiCor).

a

**5.4. Cell growth inhibitory assay.** Cells were seeded on a 96-well microplate ( $5 \times 10^2$  cells /100  $\mu$ L medium). After 24 hours, a test compound was added to them so as to be an appropriate concentration. After 168 hours incubation, 100  $\mu$ L CellTiter-Glo (G7573, Promega) was added to each well. After 20 minutes incubation, the luminescence was measured with a microplate reader (ARVO MX 1420). For nuclear count, 100  $\mu$ L CyQuant Direct nucleic acid stain (C35011, Invitrogen) was added to each well. After 1 hour incubation, the fluorescence was measured with ARVO MX 1420.

**5.5. Western blotting of phospho-STAT1.** Cell pellets and tumor samples were lysed in lysis buffer (62.5 mM Tris-Cl[pH 7.5], 1% SDS, 5% Glycerol) and were boiled at 95 °C for 5 minutes. A total of 5  $\mu$ g of protein were separated on SDS-polyacrylamidegels. Proteins were transferred with iBlot (Cat#B1001,

Invitrogen) and probed with antibodies. STAT1, Phospho-STAT1Ser727 were all purchased from Cell signaling. Secondary horseradish peroxidase-conjugated antibodies (Cell signaling) were used, and ECL plus was used to visualize the bands (LAS-3000, Fujifilm).

**5.6. Solubility.** Test compounds in DMSO solutions were added to the JP 2nd fluid for disintegration test (pH 6.8). After incubation, precipitates were separated from by filtration through a filter plate. Compound concentrations in the filtrates were measured by plate reader or HPLC.

**5.7. Microsome stability.** Human and mouse liver microsomes were purchased from Xenotech, LLC (Lenexa, KS). An incubation mixture consisted of microsomes in 50 mmol/L  $\text{KH}_2\text{PO}_4$ - $\text{K}_2\text{HPO}_4$  phosphate buffer (pH 7.4) and 1  $\mu\text{mol/L}$  test compound. The concentration of microsomal protein was 0.2 mg/mL. An NADPH-generating system (5 mmol/L  $\text{MgCl}_2$ , 5 mmol/L glucose-6-phosphate, 0.5 mmol/L beta-NADP<sup>+</sup> and 1.5 unit/mL glucose-6-phosphate dehydrogenase) was added to the incubation mixture with a half volume of the reaction mixture to initiate the enzyme reaction. The reaction was terminated 15 and 30 minutes after the initiation of the reaction by mixing the reaction mixture with acetonitrile, followed by centrifugation at 2500 rpm for 10 min. The supernatant was subjected to LC/MS/MS analysis. The metabolic velocity was calculated as the slope of the concentration-time plot. The in vitro intrinsic metabolic clearance was calculated by dividing initial metabolic velocity by the test compound concentration in the incubation mixture.

**5.8. Time-dependent CYP3A4 inhibition (TDI).** Human liver microsomes were purchased from Xenotech, LLC (Lenexa, KS). A mixture of a test compound (30  $\mu\text{M}$ ) and microsomes in phosphate buffer (pH 7.4) was preincubated at 37 °C for 0 or 60 min in the presence of an NADPH-generating system containing  $\text{MgCl}_2$ , glucose-6-phosphate,  $\beta$ -NADP<sup>+</sup>, and glucose-6-phosphate dehydrogenase. After preincubation, enzymatic activity of CYP3A4 in the incubation mixture was determined by measuring 6 $\beta$ -hydroxytestosterone in the reaction with testosterone by UPLC. The activity (% of control) for each preincubation time was calculated as follows:  $\{(\text{activity with test compound})/(\text{activity with DMSO})\} \times 100$ . The remaining activity (% remaining) after preincubation for 60 min was calculated as follows:  $\{\text{activity at 60min} (\% \text{ of control})\}/\{\text{activity at 0min} (\% \text{ of control})\} \times 100$ .

**5.9. Pharmacokinetic Studies.** Test compounds were administered intravenously (0.1 mg/kg) or orally (1 mg/kg) by cassette dosing to non-fasted mice. After administration, blood samples were collected and centrifuged to obtain the plasma fraction. The plasma samples were deproteinized by mixing with acetonitrile, followed by centrifugation. The compound concentrations in the supernatant were measured by LC/MS/MS.

**5.10. Antitumor efficacy study.** Five-week-old female C.B17/Icr-scid/scid Jcl mice purchased from CLEA Japan Inc. (Tokyo, Japan) were maintained on a 12/12 hr light/dark cycle (lights on at 7 am) with constant temperature (23  $\pm$  2 °C). Food and water were available ad libitum. RPMI-8226 cells (1 x

$10^7$  cells/100  $\mu$ L HBSS (Gibco); Matrigel (BD Biosciences); 1: 1) were injected subcutaneously into one flank of each mouse. After tumors had reached approximately 80-140 mm<sup>3</sup>, test compound (15 mg/kg, b.i.d., po or 30 mg/kg, b.i.d., po) was administered for 14 days. The tumor size was measured with a caliper twice a week, and expressed in mm<sup>3</sup> using the formula  $0.5 \times \text{length} \times \text{width}^2$ , where *a* is the largest diameter and width is largest diameter perpendicular to *a*. Body weight was measured at the same time point of the tumor measurement. Data expresses mean  $\pm$  se. All animal studies were conducted under the guidelines of the Takeda Experimental Animal Care and Use Committee.

### Acknowledgements

The authors thank Takashi Motoyaji and Akiyoshi Tani for target identification studies leading us to focus on lead compound **1**. We also would like to express our appreciation to Osamu Ujikawa, Noritaka Kuroda, Kazuaki Takami, Masanori Okaniwa, and Shiwei Guo for their helpful advice and support in organic synthesis. We also thank Yukio Toyoda for his assistance in cell Western blotting assay development, and Tsuyoshi Ishii for his useful discussion about in vitro assay development. We are also grateful to Hiroshi Miyake, Hikichi Yuichi, and Tomoyasu Ishikawa for helpful discussion and guidance in the overall execution of this research.

### Supplementary data

Supplementary data (chemical synthesis procedures, a docking experiment of **4k**, an analysis of the human kinases, a kinase selectivity profile of **4k** and western blotting of phospho-STAT1 in anti-tumor efficacy test of **4k**) associated with this article can be found in "Supplementary material (available online)".

### Abbreviations used

ADME, absorption, distribution, metabolism, and excretion; AML, acute myelogenous leukemia; AUC, area under the blood concentration time curve; b.i.d., twice a day; CDK, Cyclin-dependent kinase;  $CL_{\text{total}}$ , clearance;  $C_{\text{max}}$ , maximum drug concentration; CRC, colorectal cancer; CTD, C-terminal domain; DDI, drug-drug interaction; DMA, *N,N*-dimethylacetamide; DMAP, *N,N*-dimethyl-4-aminopyridine; DMG loop, Asp-Met-Glu loop; *F*, bioavailability; FBS, Fetal bovine serum; GST, glutathione S-transferase; HATU, O-(7-azabenzotriazol-1-yl)-*N,N,N',N'*-tetramethyluronium-hexafluorophosphat; HEPES, 4-(2-hydroxyethyl)-1-piperazineethanesulfonic acid; HOBt, 1-hydroxybenzotriazole; HTS, high-throughput screening; INF, interferon; ICR, Institute for Cancer Research; CyJohnPhos, 2-(dicyclohexylphosphino)biphenyl; MCM3, mini-chromosome maintenance 3 protein; mCPBA, *m*-chloroperoxybenzoic acid; MED, mediator complex; MRT, mean residence time; ODS, octadecyl silyl; PBS-T, phosphate buffered saline with Tween 20; PD, pharmacodynamic; PDB, protein data bank; PK, pharmacokinetic; q.d., once a day; RNAP, RNA polymerase; rt, room temperature; SBDD, structure based drug design; SPhos, dicyclohexyl(2',6'-dimethoxy-[1,1'-biphenyl]-2-yl)phosphine; STAT, signal transducers (transduction) and activator of transcription; TR-FRET, time-resolved fluorescence resonance

energy transfer;  $V_{dss}$ , steady state volume of distribution; EDC, water soluble carbodiimide (1-[3-(dimethylamino)propyl]-3-ethylcarbodiimide); XPhos, 2-dicyclohexylphosphino-2',4',6'-triisopropylbiphenyl.

## References and notes

1. (a) Galbraith, M. D.; Donner, A. J.; Espinosa, J. M. *Transcription* **2010**, *1*, 4–12. (b) Tsutsui, T.; Fukasawa, R.; Tanaka, A.; Hirose, Y.; Ohkuma, Y. *Genes Cells* **2011**, *16*, 1208–1218. (c) Rzymiski, T.; Mikula, M.; Wiklik, K.; Brzózka, K. *Biochimica et Biophysica Acta* **2015**, *1854*, 1617–1629.
2. Rickert, P.; Seghezzi, W.; Shanahan, F.; Cho, H.; Lees, E. *Oncogene* **1996**, *12*, 2631–2640.
3. (a) Nemet, J.; Jelicic, B.; Rubelj, I.; Sopta, M. *Biochimie* **2014**, *97*, 22–27. (b) Li, N.; Fassl, A.; Chick, J.; Inuzuka, H.; Li, X.; Mansour, M. R.; Liu, L.; Wang, H.; King, B.; Shaik, S.; Gutierrez, A.; Ordureau, A.; Otto, T.; Kreslavsky, T.; Baitsch, L.; Bury, L.; Meyer, C. A.; Ke, N.; Mulry, K. A.; Kluk, M. J.; Roy, M.; Kim, S.; Zhang, X.; Geng, Y.; Zagodzón, A.; Jenkinson, S.; Gale, R. E.; Linch, D. C.; Zhao, J. J.; Mullighan, C. G.; Harper, J. W.; Aster, J. C.; Aifantis, I.; Boehmer, H.; Gygi, S. P.; Wei, W.; Look, A. T.; Sicinski, P. *Nat. Cell Biol.* **2014**, *16*, 1080–1091.
4. Firestein, R.; Bass, A. J.; Kim, S. Y.; Dunn, I. F.; Silver, S. J.; Guney, I.; Freed, E.; Ligon, A. H.; Vena, N.; Ogino, S.; Chheda, M. G.; Tamayo, P.; et al. *Nature* **2008**, *455*, 547–551.
5. Allen, B. L.; Taatjes, D. J. *Nature Reviews Molecular Cell Biology* **2015**, *16*, 155–166.
6. Giovanni, C. D.; Novellino, E.; Chilin, A.; Lavecchia, A.; Marzaro, G. *Expert Opinion on Investigational Drugs* **2016**, *25*, 1215–1230.
7. Cee, V. J.; Chen, D. Y.; Lee, M. R.; Nicolaou, K. C. *Angew. Chem., Int. Ed.* **2009**, *48*, 8952–8957.
8. Roninson, I. B.; Porter, D. C.; Wentland, M. P. WO2013116786 A1, 2013.
9. (a) Mallinger, A.; Crumpler, S.; Pichowicz, M.; Waalboer, D.; Stubbs, M.; Adeniji-Popoola, O.; Wood, B.; Smith, E.; Thai, C.; Henley, A. T.; Georgi, K.; Court, W.; Hobbs, S.; Box, G.; Ortiz-Ruiz, M. J.; Valenti, M.; De Haven Brandon, A.; TePoele, R.; Leuthner, B.; Workman, P.; Aherne, W.; Poeschke, O.; Dale, T.; Wienke, D.; Esdar, C.; Rohdich, F.; Raynaud, F.; Clarke, P. A.; Eccles, S. A.; Stieber, F.; Schiemann, K.; Blagg, J. *J. Med. Chem.* **2015**, *58*, 1717–1735. (b) Mallinger, A.; Schiemann, K.; Rink, C.; Stieber, F.; Calderini, M.; Crumpler, S.; Stubbs, M.; Adeniji-Popoola, O.; Poeschke, O.; Busch, M.; Czodrowski, P.; Musil, D.; Schwarz, D.; Ortiz-Ruiz, M.; Schneider, R.; Thai, C.; Valenti, M.; Brandon, A.; Burke, R.; Workman, P.; Dale, T.; Wienke, D.; Clarke, P. A.; Esdar, C.; Raynaud, F. I.; Eccles, S. A.; Rohdich, F.; Blagg, J. *J. Med. Chem.* **2016**, *59*, 1078–1101.
10. Koehler, M. F. T.; Bergeron, P.; Blackwood, E. M.; Bowman, K.; Clark, K. R.; Firestein, R.; Kiefer, J. R.; Maskos, K.; McClelland, M. L.; Orren, L.; Salphati, L.; Schmidt, S.; Schneider, E. V.; Wu, J.; Beresini, M. H. *ACS Med. Chem. Lett.* **2016**, *7*, 223–228.
11. Schiemann, K.; Mallinger, A.; Wienke, D.; Esdar, C.; Poeschke, O.; Busch, M.; Rohdich, F.; Eccles, S. A.; Schneider, R.; Raynaud, F. I.; Czodrowski, P.; Musil, D.; Schwarz, D.; Urbahns, K.; Blagg, J. *Bioorg. Med. Chem. Lett.* **2016**, *26*, 1443–1451.
12. For previous related work, see also Ono, K.; Banno, H.; Okaniwa, M.; Hirayama, T.; Iwamura, N.; Hikichi, Y.; Murai, S.; Hasegawa, M.; Hasegawa, Y.; Yonemori, K.; Hata, A.; Aoyama, K.; Cary, D. R. *Bioorg. Med. Chem.*, submitted for publication.
13. Ujikawa, O.; Takami, K.; Takakura, N.; Sakai, N. WIPO Patent WO 2012/008549, Jan 19, 2012.
14. Based on data from UniProt Home Page. <http://www.uniprot.org/> and RSCB Protein Data Bank Home Page. <http://www.rcsb.org/pdb/> (PDB ID: 3RGF) (accessed October 31, 2016).
15. Schneider, E. V.; Böttcher, J.; Blaesche, M.; Neumann, L.; Huber, R.; Maskos, K. *J. Mol. Biol.* **2011**, *412*, 251–266.
16. Partial details of synthetic methods described in Hirayama, T.; Fujimoto, J.; Cary, D. R.; Okaniwa, M.; Hirata, Y. WIPO PCT

WO2015/159938, October 22, 2015.

17. The NMR data of the compound **22** is shown in Supplementary Figure 4.
18. Bancerek, J.; Poss, Z. C.; Steinparzer, I.; Sedlyarov, V.; Pfaffenwimmer, T.; Mikulic, I.; Dölken, L.; Strobl, B.; Müller, M.; Taatjes, D. J.; et al. *Immunity* **2013**, *38*, 250–262.
19. (a) Estrada, A. A.; Shore, D. G.; Blackwood, E.; Chen, Y.-H.; Deshmukh, G.; Ding, X.; DiPasquale, A. G.; Epler, J. A.; Friedman, L. S.; Koehler, M. F. T.; Liu, L.; Malek, S.; Nonomiya, J.; Ortwine, D. F.; Pei, Z.; Sideris, S.; St-Jean, F.; Trinh, L.; Truong, T.; Lyssikatos, J. P. *J. Med. Chem.*, **2013**, *56*, 3090–3101. (b) For a recent publication and reference regarding Bredt's Rule, see Tani, K.; Stoltz, B. M. *Nature*. **2006**, *441*, 731–734.
20. Fabian, M. A.; Biggs, W. H. 3rd; Treiber, D. K.; Atteridge, C. E.; Azimioara, M. D.; Benedetti, M. G.; Carter, T. A.; Ciceri, P.; Edeen, P.T.; Floyd, M.; Ford, J. M.; Galvin, M.; Gerlach, J. L.; Grotzfeld, R. M.; Herrgard, S.; Insko, D. E.; Insko, M. A.; Lai, A. G.; Lélías, J. M.; Mehta, S. A.; Milanov, Z. V.; Velasco, A. M.; Wodicka, L. M.; Patel, H. K.; Zarrinkar, P. P.; Lockhart, D. J. *Nat. Biotechnol.* **2005**, *23*, 329–336.

